© 2017. Published by The Company of Biologists Ltd | Journal of Cell Science (2017) 130, 1450-1462 doi:10.1242/jcs.196832

RESEARCH ARTICLE

The centriolar satellite protein CCDC66 interacts with CEP290 and functions in cilium formation and trafficking

Deniz Conkar[1], Efraim Culfa[1], Ezgi Odabasi[1], Navin Rauniyar[2], John R. Yates, III[2] and Elif N. Firat-Karalar[1,*]

ABSTRACT

Centriolar satellites are membrane-less structures that localize and move around the centrosome and cilium complex in a microtubule-dependent manner. They play important roles in centrosome- and cilium-related processes, including protein trafficking to the centrosome and cilium complex, and ciliogenesis, and they are implicated in ciliopathies. Despite the important regulatory roles of centriolar satellites in the assembly and function of the centrosome and cilium complex, the molecular mechanisms of their functions remain poorly understood. To dissect the mechanism for their regulatory roles during ciliogenesis, we performed an analysis to determine the proteins that localize in close proximity to the satellite protein CEP72, among which was the retinal degeneration gene product CCDC66. We identified CCDC66 as a microtubule-associated protein that dynamically localizes to the centrosome, centriolar satellites and the primary cilium throughout the cell cycle. Like the BBSome component BBS4, CCDC66 distributes between satellites and the primary cilium during ciliogenesis. CCDC66 has extensive proximity interactions with centrosome and centriolar satellite proteins, and co-immunoprecipitation experiments revealed interactions between CCDC66, CEP290 and PCM1. Ciliogenesis, ciliary recruitment of BBS4 and centriolar satellite organization are impaired in cells depleted for CCDC66. Taken together, our findings identify CCDC66 as a targeting factor for centrosome and cilium proteins.

KEY WORDS: CCDC66, Centriolar satellites, Ciliogenesis, Centrosome, BioID proximity mapping, BBS4

INTRODUCTION

Centrosomes are main microtubule-organizing centers of animal cells. They create various microtubule arrays, and thus influence cell shape, polarity and motility, as well as spindle formation, chromosome segregation and cell division (Luders and Stearns, 2007). Centrosomes are composed of two cylindrical microtubule-based structures termed centrioles and associated pericentriolar material (PCM) that nucleates and organizes microtubules. Importantly, centrioles nucleate the formation of the primary cilium, which functions as a hub for developmentally important signaling pathways including Hedgehog, Wnt and platelet-derived growth factor receptor-α pathways (Berbari et al., 2009; Kim and Dynlacht, 2013). In addition to centrioles and PCM, vertebrate cells have an array of 70–100 nm membrane-less structures that localize and move around the centrosome and cilium complex in a microtubule- and molecular motor-dependent manner, termed "centriolar satellites' (Barenz et al., 2011; Tollenaere et al., 2015).

Importantly, there are many links between the centrosome and cilium complex and human disease (Bettencourt-Dias et al., 2011; Nigg and Raff, 2009). Abnormalities of centrosome structure and number have long been associated with cancer (Vitre and Cleveland, 2012). Moreover, mutations affecting components of the centrosome and cilium complex and satellites cause a set of disease syndromes termed ciliopathies, which are characterized by a diverse set of phenotypes, including renal disease, retinal degeneration, polydactyly, neurocognitive deficits and obesity (Adams et al., 2007; Hildebrandt et al., 2011). Although more than 40 genes have been identified as causative genes for ciliopathies, the underlying molecular mechanisms of these disease syndromes remains poorly understood (Waters and Beales, 2011). To determine these mechanisms, it is important to dissect the underlying factors that regulate the assembly and function of the centrosome and cilium complex.

Emerging evidence has revealed important regulatory functions for the centriolar satellites in the assembly and function of the centrosome and cilium complex. Centriolar satellite proteins identified so far play important roles in various processes such as cilium formation (Wang et al., 2016), centrosome duplication (Firat-Karalar et al., 2014; Kodani et al., 2015), microtubule organization, mitotic spindle formation (Kim and Rhee, 2011), chromosome segregation (Kim et al., 2012; Staples et al., 2012), the stress response (Villumsen et al., 2013), autophagy (Pampliega et al., 2013; Tang et al., 2013) and neurogenesis (Tollenaere et al., 2015). Interestingly, a significant percentage of satellite components also localize to the centrosome and cilium complex (Tollenaere et al., 2015). Moreover, all satellite-linked diseases including ciliopathies, primary microcephaly and various neurological disorders are also associated with abnormalities of the centrosome and cilium complex (Kodani et al., 2015; Tollenaere et al., 2015). These lines of evidence together suggest that satellites are ubiquitous and essential structures for the centrosome and cilium complex in vertebrates. However, the molecular mechanism of how the centrosome and cilium complex is regulated by centriolar satellites remains poorly understood.

Centriolar satellites play important roles during cilium assembly and function, most likely by trafficking proteins to or away from the centrosome and cilium complex or sequestering them (Tollenaere et al., 2015). Among the proteins that localize to centriolar satellites are the ciliopathy proteins CEP290 and BBS4, which function in the highly regulated trafficking of ciliary proteins into and out of the cilium. CEP290 is a component of the transition zone that forms a selective barrier at the base of the cilium (Betleja and Cole, 2010). BBS4 is one of the seven highly conserved Bardet–Biedl syndrome (BBS) proteins that together form a coat complex and traffic

[1]Department of Molecular Biology and Genetics, Koç University, Istanbul 34450, Turkey. [2]Department of Chemical Biology, The Scripps Research Institute, 10550 N. Torrey Pines Rd., La Jolla, CA 92037, USA.

*Author for correspondence (ekaralar@ku.edu.tr)

E.N.F., 0000-0001-7589-473X

Received 22 August 2016; Accepted 16 February 2017

Journal of Cell Science

Journal of Cell Science (2017) 130, 1450-1462 doi:10.1242/jcs.196832

membrane proteins to cilia (Nachury, 2008; Nachury et al., 2007). In addition to the transition zone and the BBSome complex, intraflagellar transport proteins are also critical for ciliary trafficking, as they function in the bidirectional movement of multiprotein complexes along the axoneme (Scholey, 2008). Ciliary protein trafficking is key to the formation and function of the primary cilium, and impaired ciliary trafficking is a significant defect associated with ciliopathies.

To elucidate the molecular mechanism of how centriolar satellites regulate cilium assembly and function, it is important to identify the full repertoire of satellite proteins. To this end, we have started building a proximity interaction map for satellite proteins implicated in cilium assembly and function. The interactors identified by this map include both known satellite proteins and previously uncharacterized proteins (Firat-Karalar et al., 2014). Among these proteins, we chose CCDC66, for further study, because it has been previously implicated in microtubule-mediated functions, including spindle pole and centriolar satellite organization (Gupta et al., 2015; Sharp et al., 2011), and its link to retinal degeneration (Dekomien et al., 2010; Gerding et al., 2011). A homozygous mutation in the *CCDC66* gene was shown to cause autosomal recessively inherited, generalized progressive retinal atrophy, the canine counterpart of Retinitis pigmentosa (Dekomien et al., 2010). Moreover, *CCDC66* knockout in mouse leads to early photoreceptor degeneration, with a slow, progressive retinal phenotype and physiological impairment of the retina (Gerding et al., 2011). These studies together suggest an important role for CCDC66 in retinal development and function.

In this study, we functionally and biochemically characterized CCDC66 in ciliated RPE1 cells. We showed that CCDC66 localizes to the centrosome and the centriolar satellites. Strikingly, CCDC66 redistributes between centriolar satellites and the primary cilium in ciliated cells, which identifies CCDC66 as the only protein other than BBS4 with such relocalization pattern. CCDC66 binds to microtubules *in vitro* and *in vivo* and, when overexpressed, it bundles microtubules, disrupts the cellular distribution of centriolar satellites and inhibits ciliogenesis. BioID proximity mapping of CCDC66, but not the CCDC66 deletion mutant that mimics the truncated protein described in retinal degeneration, revealed extensive interactions with centrosome and satellite proteins. In agreement with these interactions, CCDC66 colocalizes and interacts with the satellite proteins PCM1 and CEP290 and functions in cilium formation, satellite organization and BBS4 recruitment to the primary cilium. Taken together, our findings identify a critical function of CCDC66 in cilium formation and a possible function in ciliary trafficking.

RESULTS

Proximity mapping identifies new centriolar satellite proteins

To identify new components of centriolar satellites that function during ciliogenesis, we determined the proteins that localized in close proximity to CEP72 at the centriolar satellites by using the BioID approach (Firat-Karalar and Stearns, 2015; Roux et al., 2013). CEP72 localizes to centriolar satellites and interacts with CEP290 to recruit BBS proteins to the primary cilium (Stowe et al., 2012). We generated an N-terminal Myc–BirA (R118G) promiscuous biotin ligase (hereafter BirA*) fusion of CEP72 and showed that Myc–BirA*–CEP72 (hereafter BirA*–CEP72) localized to the centriolar satellites, as assessed by anti-Myc staining (Fig. S1A) and stimulated localized biotinylation of the centriolar satellites, as assessed by streptavidin staining (Fig. 1A). HEK293T cells were then transfected with BirA*–CEP72, supplemented with 50 µM biotin 24 h post transfection, and incubated for 18 h. After cells were solubilized with denaturing lysis buffer, biotinylated proteins were precipitated with streptavidin beads and analyzed by mass spectrometry. HEK293T cells transfected with BirA*, or mock-transfected, were processed in parallel as controls. The interactors identified (hereafter referred to as proximity interactors) for CEP72 are listed by their normalized spectral abundance factor (NSAF) value in Fig. 1B and Table S1. The NSAF value is an estimate of relative abundance of proteins in a sample. A significant percentage of the proximity interactors of CEP72 are centrosome and/or centriolar satellite components, validating the power of our approach to identify proximity interactors at the centriolar satellites. The CEP72 BioID hits also include proteins that were not previously implicated in ciliogenesis. Among these hits is the retinal degeneration gene *CCDC66* (Dekomien et al., 2010; Gerding et al., 2011). CCDC66 has been reported to localize to centriolar satellites (Gupta et al., 2015) and its mRNA has been found to interact with microtubules in a screen for microtubule-binding transcripts in *Xenopus laevis* egg extracts (Sharp et al., 2011). CCDC66 was also previously identified a proximity partner of the canonical satellite protein PCM1 (Gupta et al., 2015), but not for CCDC14 and KIAA0753, which regulate centriole duplication (Firat-Karalar and Stearns, 2015). Based on its proximity to regulators of ciliogenesis, disease link and cellular localization, we chose CCDC66 for further study.

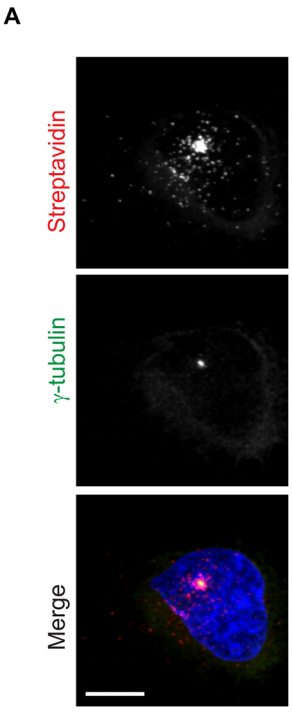

B

BirA*-CEP72

Protein	NSAF
CEP72	500
UBB	10.74
SKA3	6.68
CEP55	3.55
TTC1	3.28
CEP85	2.47
CSPP1	2.20
PLK1S1	1.90
LZTS2	1.84
OFD1	1.71
PCM1	1.60
AZI1	1.48
ABLIM1	1.35
CEP90	1.24
SSX2IP	1.24
CEP290	1.01
MPHOSPH9	1.00
CCDC93	0.96
FAM184A	0.81
CCDC66	0.80
GTSE1	0.74
GRINL1A	0.72
FAM21B	0.59
CCDC15	0.56
SYNM	0.50

Fig. 1. Localization, activity and proximity interactors of BirA*-tagged CEP72. (A) BirA*–CEP72 stimulates biotinylation at the centriolar satellites. RPE1 cells were transfected with Myc–BirA*-tagged CEP72. After 18 h incubation with biotin, cells were fixed and stained for biotinylated proteins with fluorescent streptavidin and for centrosomes with anti-γ-tubulin antibody. DNA was stained with DAPI. Scale bar: 10 µm. (B) Mass spectrometry analysis of proximity interactors of Myc–BirA*–CEP72. Proximity interactors are ranked in the order of their normalized spectral abundance factor (NSAF) values (mean of three independent experiments). Proteins in black were previously shown to localize to the centrosome and cilium complex, proteins in bold were previously shown to interact physically with CEP72, and proteins in grey were not associated with the centrosome and cilium complex in previous studies.

Journal of Cell Science (2017) 130, 1450-1462 doi:10.1242/jcs.196832

CCDC66 localizes to the centrosome or cilium complex and the centriolar satellites

To gain insight into the molecular mechanism of satellite function during ciliogenesis, we characterized CCDC66 in ciliated hTERT-RPE1 (hereafter RPE1) cells. Orthologs of CCDC66 are present in hemichordates and placozoans but absent in arthropods, nematodes and Chlamydomonas. The evolutionary conservation pattern of CCDC66 is similar to that of the core centriolar satellite protein PCM1 (Hodges et al., 2010) but not BBS4 (Kim et al., 2004) and CEP290 (Kim et al., 2008). CCDC66 contains two coiled-coil (CC) domains: CC1 (amino acids 252–283) and CC2 (amino acids 466–564) and an evolutionarily conserved CCDC66 domain (Pfam 15236) (amino acids 408–564), part of which overlaps with CC2 (see Fig. 4).

Expression studies in dog and mouse tissues via quantitative real-time RT-PCR (qRT-PCR) (Dekomien et al., 2010) and a genome-wide analysis of transcription profiles (Krupp et al., 2012) showed that CCDC66 is not only expressed in retina but most tissues including heart, brain, liver and blood. Immunoblotting with an antibody against CCDC66 in RPE1, HeLa and HEK293T cell extracts validated the wide expression profile of CCDC66 (Fig. 2A).

We examined the localization of endogenous CCDC66 and a GFP–CCDC66 fusion protein in RPE1 cells. Antibody against endogenous CCDC66 revealed that it localizes to the centrosome and centriolar satellites in interphase cells, as assessed by colocalization with PCM1, a marker for the centriolar satellites and γ-tubulin, a marker for the centrosome (Fig. 2B). A similar localization to the centrosome and centriolar satellites (Fig. S1C) was observed in RPE1 cells stably expressing GFP–CCDC66 fusion protein at near-endogenous level (Fig. S1B).

The punctate pericentrosomal distribution of satellite proteins is dependent on PCM1, a centrosomally focused microtubule array and the microtubule motor dynein (Kim et al., 2008, 2004; Lopes et al., 2011). Upon depolymerization of microtubules, the centriolar satellite pool of CCDC66 dispersed throughout the cytoplasm (Fig. 2B), as expected for centriolar satellites. Moreover, depletion of PCM1 caused loss of CCDC66 satellite localization (Fig. 2B). In both cases CCDC66 remained associated with the centrosome (Fig. 2B). These results show that the CCDC66-containing foci are canonical centriolar satellites and that CCDC66 localizes to the centrosome in addition to the centriolar satellites. In agreement, immunostaining of centrosomes purified from HEK293T cells with CCDC66 revealed colocalization with γ-tubulin and centrin (Fig. 2D).

CCDC66 localizes to the centriolar satellites and the centrosome during centriole duplication and growth in S and G2 phases (Fig. S1C). However, its localization becomes restricted to the centrosomes and the spindle microtubules during mitosis (Fig. 2E; Fig. S1C,D). Live-imaging of RPE1 cells stably expressing GFP–CCDC66 revealed dynamic distribution of CCDC66 between the centrosome, centriolar satellites and microtubules throughout the cell cycle (Fig. 2F; Fig. S1E, Movies 1, 2), consistent with the localization of endogenous CCDC66. Such dynamic behavior is similar to the localization of other satellite proteins including CEP290, CCDC11, FOP (also known as FGFR1OP) and CCDC13 (Kim et al., 2008; Lee and Stearns, 2013; Silva et al., 2016; Staples et al., 2014).

To assess the localization of CCDC66 upon primary cilium assembly, RPE1 cells stably expressing GFP–CCDC66 were serum-starved for 48 h. In most non-ciliated serum-starved cells, the satellite pool of GFP–CCDC66 diminished significantly and GFP–CCDC66 localized prominently to the centrosome (Fig. 2C). Remarkably, in 95±4.5% of ciliated cells (mean±s.e.m.; n=500) GFP–CCDC66 redistributed from centriolar satellites to the primary cilium and basal body (Fig. 2G,H), in an analogous manner to the movement of the BBSome complex component BBS4 (Nachury et al., 2007). In the remaining cells, GFP–CCDC66 localized to the cilium, basal body and centriolar satellites (Fig. 2G,H). In ciliated cells, GFP–CCDC66 colocalized with PCM1 and CEP290 at the centriolar satellites, and with poly-glutamylated tubulin at the primary cilium and the basal body (Fig. 2G,H). We did not observe CCDC66 localization at the ciliary transition zone, as assessed by staining with CEP290 (Fig. 2H). Of note, we did not detect localization of CCDC66 to the primary cilium of RPE1 cells using the current antibodies, which is likely due to the technical difficulties in the fixation and processing of intraciliary antigens (Follit et al., 2006; Nachury et al., 2007). These results identify CCDC66 as the only protein other than BBS4 that has so far been identified to redistribute between centriolar satellite and ciliary pools in ciliated cells.

Analysis of CCDC66 deletion mutants for localization to the centriolar satellites and the centrosome

To identify the functionally important domains of CCDC66 for localization to centriolar satellites and the centrosome, we generated a series of GFP-tagged CCDC66 deletion mutants (Fig. 4). GFP–CCDC66 truncations lacking the conserved CCDC66 region failed to localize to satellites and the centrosome, and instead had diffuse cytoplasmic and/or nuclear distribution, except for GFP–CCDC66 (564–948), which colocalized with γ-tubulin (Fig. S2A,B). The conserved CCDC66 region did not localize to centriolar satellites and the centrosome by itself (Fig. S2A,B). These data suggest that more than one region of CCDC66 is required for its localization to the centrosome and the satellites. GFP–CCDC66 (408–948) colocalized with PCM1-positive puncta in transfected cells, in which the distribution of satellites changed, possibly due to changes in the organization of microtubules (Fig. S2B). The deletion mutant CCDC66-RD (amino acids 1–207) mimics the truncated protein described in the dogs with a point mutation in CCDC66, which causes a frameshift that introduces a premature stop codon at amino acid 207 (Dekomien et al., 2010). Interestingly, CCDC66-RD localizes diffusely throughout the cytoplasm and nucleus (Fig. S2), suggesting that retinal degeneration phenotype might result from disruption of the localization and interactions of CCDC66 in cells.

CCDC66 is a microtubule-associated protein

CCDC66 mRNA was previously shown to associate with microtubules in a screen for microtubule-binding mRNAs in *Xenopus laevis* eggs (Sharp et al., 2011), suggesting a possible function for CCDC66 in microtubule-based cellular processes. To address this possibility, we examined the affinity of CCDC66 to microtubules using *in vitro* and *in vivo* assays. In transiently transfected high-expressing cells, GFP–CCDC66 localized to microtubules (Fig. 3A). Interestingly, we found that 67±6.3% of transfected cells (mean±s.e.m.; n=200) had microtubule bundles, which was not observed in control cells transfected with GFP. In a subset of cells, the microtubule bundles were associated with the centrosome and stained for α-tubulin and PCM1, but did not stain for the ciliary axoneme marker poly-glutamylated tubulin, suggesting that they are not normal cilia (Fig. 3B). Although GFP–CCDC66 overexpression induced microtubule bundles, there was no significant change (P=0.58) in the total fluorescence intensity of α-tubulin between GFP–CCDC66-expressing cells and control GFP-expressing cells.

Journal of Cell Science

Journal of Cell Science (2017) 130, 1450-1462 doi:10.1242/jcs.196832

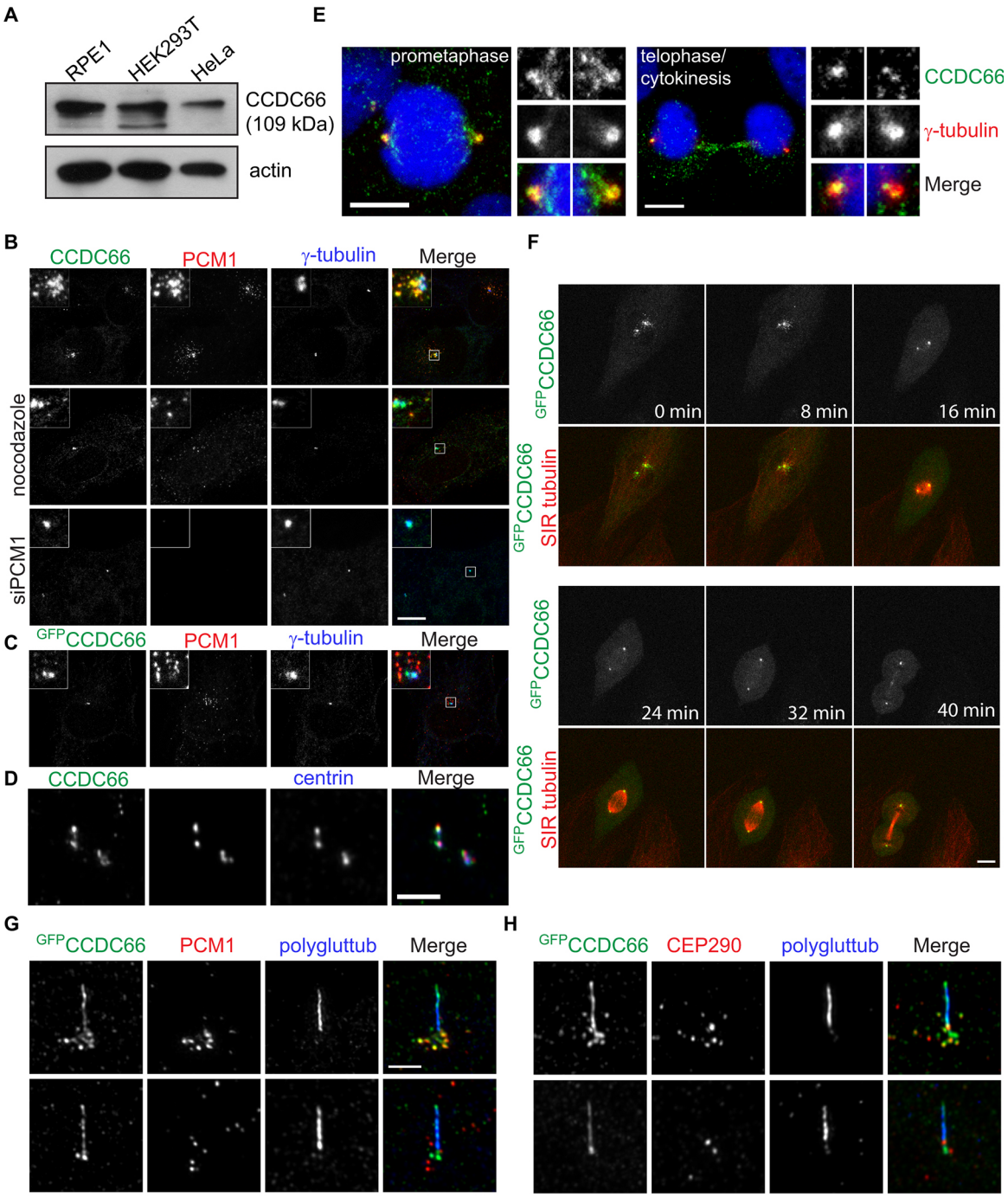

Fig. 2. CCDC66 expression and localization in cultured RPE1 cell line. (A) CCDC66 is expressed in various mammalian cell lines. Extracts from RPE1, HEK293T and HeLa cells were blotted for CCDC66 and actin (loading control). (B) Localization of endogenous CCDC66 in interphase, nocodazole-treated cells and PCM1-depleted (siPCM1) cells. RPE1 cells were fixed and stained for CCDC66, PCM1 and γ-tubulin. To determine the effect of microtubule depolymerization on CCDC66 localization, RPE1 cells were treated with 10 µg/ml nocodazole for 3 h, fixed and stained for GFP, PCM1 and γ-tubulin. To determine the effect of PCM1 depletion on CCDC66 localization, RPE1 cells were fixed 48 h after transfection with control PCM1 siRNA, fixed and stained. (C) Localization of GFP–CCDC66 (^{GFP}CCDC66) in serum-starved non-ciliated RPE1 cells stably expressing GFP–CCDC66, which were fixed and stained for CCDC66, PCM1 and γ-tubulin. (D) Localization of CCDC66 to purified centrosomes. Purified centrosomes were spun down on coverslips, fixed and stained for CCDC66, γ-tubulin and centrin. (E) Localization of endogenous CCDC66 in prometaphase and telophase/cytokinesis stages of the cell cycle. Asynchronously growing RPE1 cells were fixed and stained for CCDC66 and γ-tubulin. DNA was stained with DAPI. Scale bars: 10 µm, all insets show 4× enlarged centrosomes. (F) Dynamic localization of GFP–CCDC66 throughout the cell cycle. Shown are six time-lapse images of a dividing cell. See Movie 1. (G,H) Localization of CCDC66 in ciliated cells. RPE1 cells stably expressing GFP–CCDC66 were fixed 48 h after serum starvation and stained for (G) GFP, PCM1 and glutamylated tubulin and (H) GFP, CEP290 and glutamylated tubulin. Images represent deconvolved maximum projection of sections. Scale bars: 2.5 µm. ^{GFP}CCDC66 indicates stable expression of the fusion protein.

Given the association of CCDC66 with microtubules *in vivo*, we next studied whether CCDC66 interacts with microtubules using *in vitro* microtubule pelleting assays. We first performed the pelleting assays with lysates from cells transfected with GFP–CCDC66 or GFP as a negative control. In agreement with the localization results, GFP–CCDC66, but not GFP, co-pelleted with

Journal of Cell Science (2017) 130, 1450-1462 doi:10.1242/jcs.196832

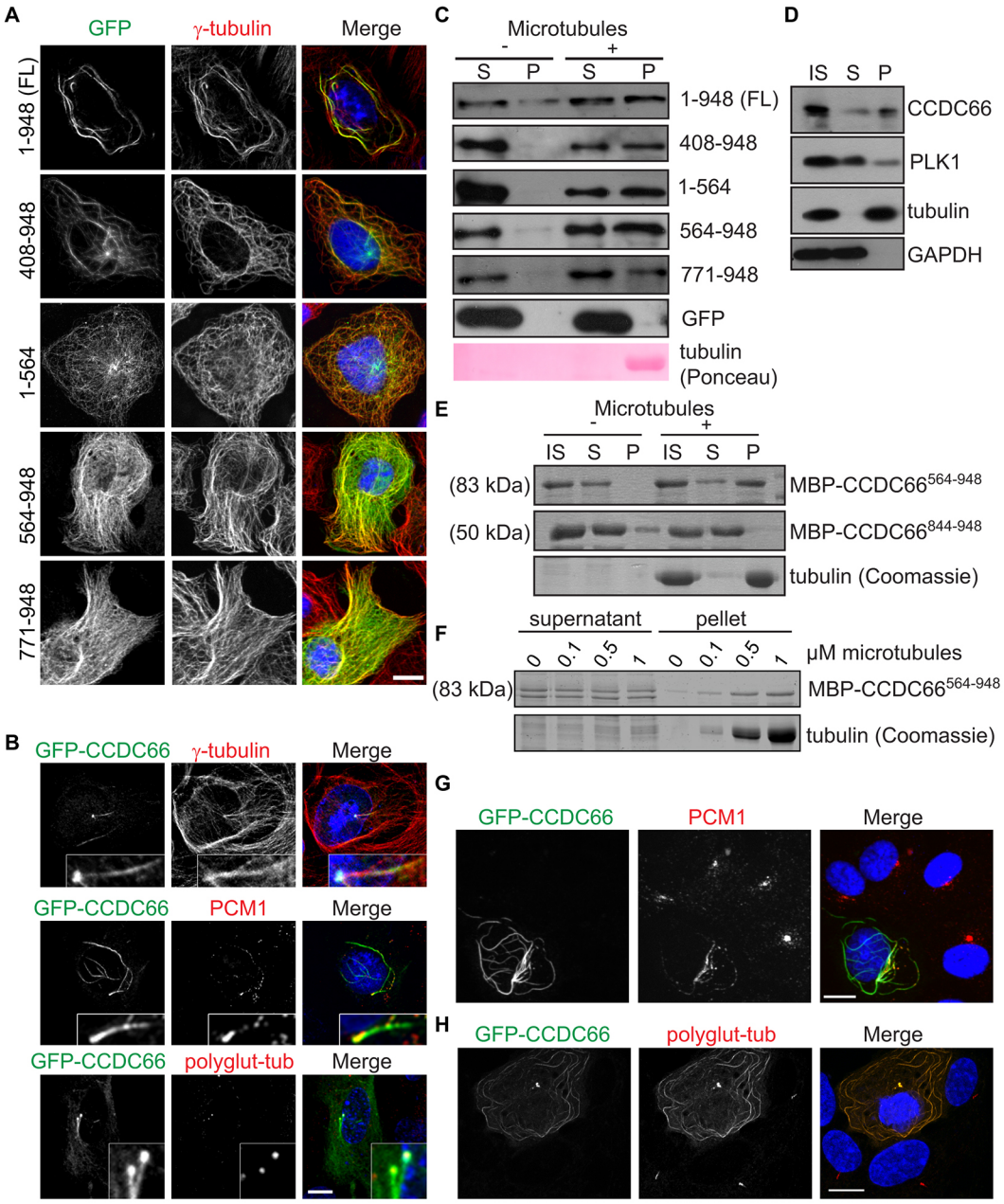

Fig. 3. CCDC66 is a microtubule-associated protein. (A) GFP–CCDC66 localizes to microtubules in transiently transfected cells. RPE1 cells transfected with GFP-tagged full-length CCDC66 and its deletion constructs were fixed and stained for GFP and α-tubulin. (B) The bundles associated with the centrosome colocalize with α-tubulin and PCM1. RPE1 cells transiently transfected with GFP–CCDC66 were fixed and stained for GFP and α-tubulin, glutamylated tubulin or PCM1. (C–E) CCDC66 binds to microtubules *in vitro*. Microtubule pelleting assays were performed using (C) extracts from cells expressing GFP-tagged full-length CCDC66 and its deletion constructs or (D) extracts from untransfected cells or (E) 0.5 nmol purified MBP-tagged CCDC66 fragments. Indicated cell extracts or purified proteins were incubated with taxol-stabilized microtubules or buffer, loaded onto a 40% glycerol cushion and spun down. Initial sample (IS), Supernatant (S) and pellet (P) fractions were blotted for GFP, CCDC66, PLK1 (positive control), GAPDH (negative control) or tubulin. Microtubules were detected using Ponceau stain in C and D. Proteins were detected using Coomassie blue stain in E. (F) MBP–CCDC66 (564–948) ($MBP\text{-}CCDC66^{564\text{-}948}$) binds to microtubules. 0.5 nmol MBP–CCDC66 (564–948) was incubated with increasing amounts of taxol-stabilized microtubules, loaded onto a 40% glycerol cushion and spun down. Supernatant and pellet fractions were resolved by SDS–PAGE and proteins were detected using Coomassie blue stain. (G) CCDC66 overexpression disrupts organization of centriolar satellites. RPE1 cells transiently transfected with GFP–CCDC66 were fixed and stained for GFP and PCM1. (H) GFP–CCDC66 overexpression inhibits ciliogenesis. Ciliation was induced in GFP–CCDC66-transfected RPE1 cells by serum starvation for 24 h. Cells were fixed and stained for GFP and polyglutamylated tubulin. DNA was stained with DAPI. Scale bars: 10 μm.

taxol-stabilized microtubules (Fig. 3C). To determine whether endogenous CCDC66 also interacts with microtubules and that the interaction of GFP–CCDC66 to microtubules is not a consequence of overexpression, we performed *in vitro* microtubule pelleting assays with cell lysates and demonstrated that endogenous CCDC66 co-pellets with taxol-stabilized microtubules (Fig. 3D). As control, the cytoplasmic protein GAPDH remained in the supernatant, whereas the microtubule-associated protein PLK1 co-pelleted with microtubules (Fig. 3D). The affinity of endogenous CCDC66 to microtubules is consistent with the localization of

Journal of Cell Science (2017) 130, 1450-1462 doi:10.1242/jcs.196832

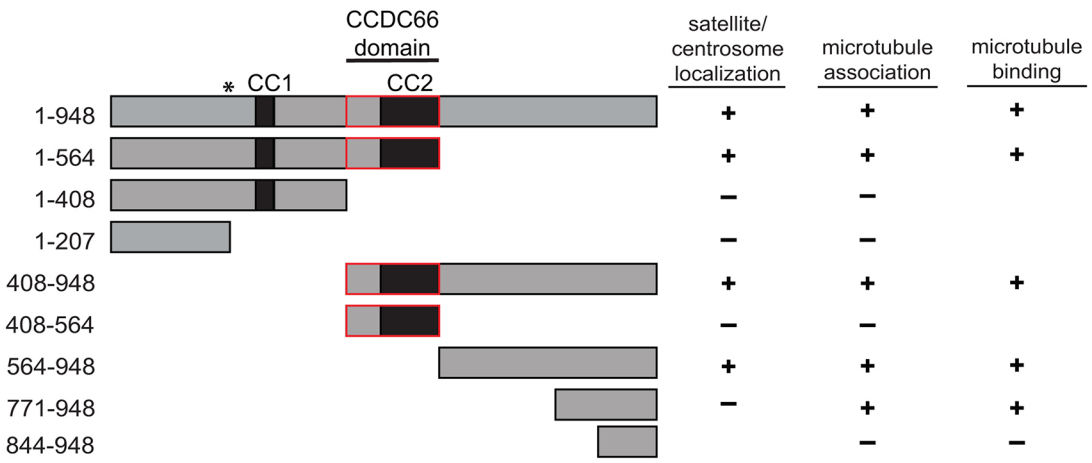

Fig. 4. Localization and interaction analysis of CCDC66 deletion mutants. Schematic representation of CCDC66 full length (FL) and deletion constructs and summary of their localization to centriolar satellites and the centrosome, and their interaction or association with microtubules. Satellite and centrosome localization and microtubule association were determined by analyzing RPE1 cells transiently transfected with GFP–CCDC66 constructs and staining fixed cells for GFP and PCM1, γ-tubulin or microtubules. Microtubule binding was determined by *in vitro* microtubule pelleting assays of extracts from cells transiently expressing GFP-tagged full-length CCDC66 and its deletion constructs and/or purified proteins. Numbers indicate amino acid positions, CC1 and CC2 indicate coiled coil domains and 'CCDC66 domain' indicates the conserved domain in CCDC66 orthologs. The asterisk indicates the point mutation at amino acid 207 in in dogs with retinal degeneration. CCDC66 (1-207) deletion mutant represents the CCDC66-RD (retinal degeneration) mutant.

CCDC66 to the spindle microtubules and mid-zone during mitosis (Fig. 2E; Fig. S1D).

To identify the regions of CCDC66 that are important for microtubule association and binding, we determined the localization of these mutants in transfected cells (Fig. 3A; Fig. S3A) and tested whether the GFP-tagged CCDC66 truncation mutants that are positive for microtubule association bind to microtubules using the *in vitro* microtubule pelleting assays (Fig. 3C). The N-terminal 564 amino acids, containing the CCDC66 conserved region and the C-terminal 177 amino acids localized and interacted with microtubules (Fig. 4). Interestingly, expression of these fragments did not induce formation of microtubule bundles, instead they decorated the microtubule network in cells (Fig. 3A). These data suggest that two different regions mediate CCDC66 interaction with microtubules and that only the full-length protein can change the organization of microtubule network through bundling.

To test whether association of CCDC66 with microtubules reflects direct binding, we purified recombinant MBP-tagged CCDC66 (564-948) and CCDC66 (844-948) and performed an *in vitro* microtubule pelleting assays. Consistent of with the localization results, the microtubule-binding MBP–CCDC66 (564-948), but not the negative control MBP–CCDC66 (844-948) pelleted with microtubules (Fig. 3E; Fig. S3B). The fraction of MBP–CCDC66 (564-948) in the pellet increased with increasing concentrations of taxol-stabilized microtubules (Fig. 3F). Taken together, these data indicate a direct interaction of CCDC66 with microtubules and identify CCDC66 as a microtubule-associated protein.

Overexpression of CCDC66 disrupts organization of centriolar satellites and inhibits primary cilium formation

Overexpression of centriolar satellite proteins CEP290 and BBS4 disrupts centriolar satellite distribution by forming aggregates that sequester PCM1 (Kim et al., 2008, 2004). Unlike CEP290 and BBS4 and most other centriolar satellites proteins, we did not observe formation of cytoplasmic aggregates upon overexpression of CCDC66 (Fig. 3A). In highly expressing cells, GFP–CCDC66 formed cytoplasmic microtubule bundles that sequestered endogenous PCM1, with a corresponding reduction in pericentrosomally distributed centriolar satellites (Fig. 3G). Because the punctate pericentrosomal distribution of centriolar satellites depends on an intact microtubule network, these results suggest that GFP–CCDC66 disrupts the centriolar satellite organization through inducing microtubule bundle formation. In serum-starved RPE1 cells, overexpression of GFP–CCDC66 completely inhibited primary cilium formation (n=100), while control untransfected cells (66±5.6%, n=150) and GFP-expressing cells (52±5.6%, n=150) were efficiently ciliated (Fig. 3H).

CCDC66 interacts with the centriolar satellite proteins CEP290 and PCM1

To gain insight into the cellular functions of CCDC66, we identified its proximity interactors at the centriolar satellites by using the BioID approach (Firat-Karalar and Stearns, 2015). We generated an N-terminal Myc–BirA* fusion of CCDC66 and showed that Myc–BirA*–CCDC66 (hereafter BirA*–CCDC66) localized to centriolar satellites and stimulated localized biotinylation of the centriolar satellites, as assessed by streptavidin staining (Fig. 5A). HEK293T cells were then transfected with BirA*–CCDC66 and processed for pulldown of biotinylated proteins as for BirA*–CEP72.

The proximity interactors for CCDC66 are listed by NSAF value in Fig. 5B and Table S1. A significant percentage of proximity interactors are centrosome and/or centriolar satellite components and microtubule-associated proteins. Several of the proteins identified as proximity interactors for CCDC66 stand out by their known relationship to satellites and/or their involvement in primary cilium formation. CEP290 localizes to centriolar satellites and functions together with CEP72 during relocalization of BBS4 from centriolar satellites to primary cilia during ciliogenesis (Stowe et al., 2012). CEP162, a distal appendage protein, like CCDC66, binds to microtubules and functions in ciliogenesis (Wang et al., 2013). Other proximity interactors include PCM1, which is the scaffolding protein for satellites, AZI1 (also known as CEP131), which functions during ciliogenesis (Hall et al., 2013) and CEP55,

Journal of Cell Science (2017) 130, 1450-1462 doi:10.1242/jcs.196832

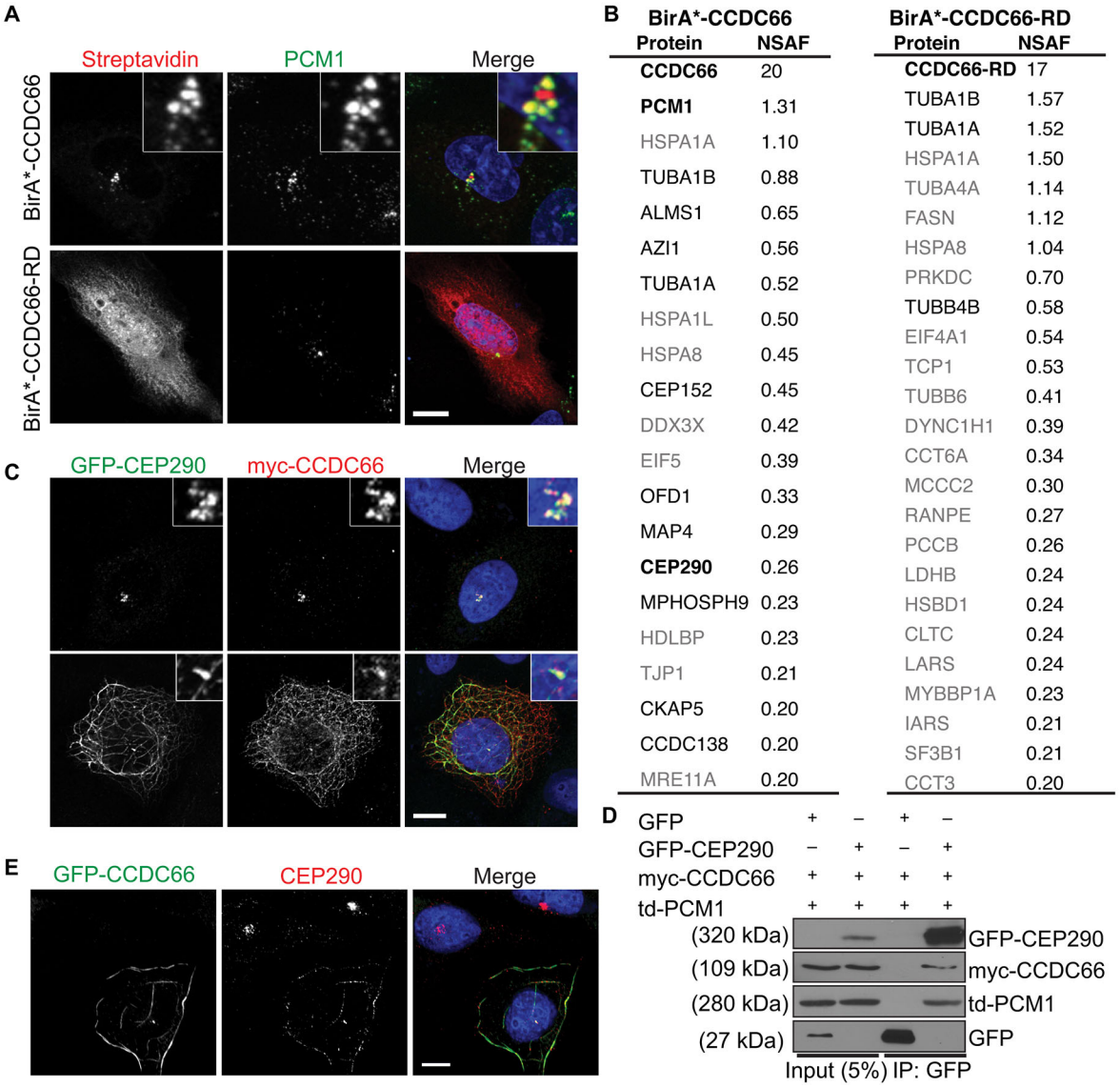

Fig. 5. Localization, activity and proximity interactors of BirA*-tagged CCDC66 and CCDC66-RD. (A) RPE1 cells were transiently transfected with Myc–BirA*-tagged CCDC66 and CCDC66-RD. After 18 h of biotin incubation, cells were fixed and stained for biotinylated proteins with fluorescent streptavidin and for centriolar satellites with anti-PCM1 antibody. DNA was stained with DAPI. Scale bar: 10 µm, inset shows 4× enlarged centrosomes. (B) Mass spectrometry analysis of proximity interactors of Myc–BirA*–CCDC66 and Myc–BirA*–CCDC66-RD. Proximity interactors are ranked in the order of their NSAF values (mean of three independent experiments). Proteins in black were previously shown to localize to the centrosome, proteins in bold were previously shown to interact physically with CCDC66 and proteins in grey were not associated with the centrosome and cilium complex in previous studies. (C) CCDC66 and CEP290 colocalize at the centriolar satellites and microtubules. RPE1 cells transiently expressing GFP–CEP290 and Myc–CCDC66 were stained with anti-Myc and anti-GFP antibodies. DNA was stained with DAPI. Scale bar: 10 µm, all insets show 4× enlarged centrosomes. (D) Co-immunoprecipitation of GFP–CEP290, tomato (td)–PCM1 and Myc–CCDC66 after co-expression in HEK293T cells. Complexes were immunoprecipitated with anti-GFP antibody and co-precipitated (IP) proteins were detected with anti-GFP, anti-Myc and anti-PCM1 antibodies. (E) GFP–CCDC66 recruits CEP290 to microtubules. RPE1 cells transiently expressing GFP–CCDC66 were stained with anti-GFP and anti-CEP290 antibodies. DNA was stained with DAPI. Scale bar: 10 µm.

which functions during cytokinesis (Martinez-Garay et al., 2006; van der Horst et al., 2009). Although we identified CCDC66 as a proximity partner for CEP72, we failed to identify CEP72 as a proximity partner for CCDC66, which could be due to differences in their relative abundance or the amount of time CCDC66 spends in its different cellular pools.

To determine which proximity interactions reflect physical association, we performed co-immunoprecipitation experiments in HEK293T cells. CCDC66 interacted with both CEP290 and PCM1 (Fig. 5D). Consistent with its interaction with CEP290, Myc–CCDC66 colocalized with GFP–CEP290 at centriolar satellites and microtubules (Fig. 5C). Interestingly, like CEP162, the microtubule bundles induced by overexpression of CCDC66 sequestered endogenous CEP290 (Fig. 5E), suggesting that CEP290 might associate with microtubules through CCDC66 (Wang et al., 2013). Although CCDC66 was initially identified as a proximity partner for CEP72, this proximity interaction did not reflect a physical interaction in in co-immunoprecipitation experiments (Fig. S3C).

A point mutation in the CCDC66 gene was implicated in retinal degeneration (Dekomien et al., 2010), but its effect on CCDC66 function has not yet been characterized. To gain insight into the molecular defects caused by this mutation, we identified the proximity interactors of the CCDC66-RD mutant and compared them with those of CCDC66. Myc–BirA*–CCDC66-RD localizes

Journal of Cell Science (2017) 130, 1450-1462 doi:10.1242/jcs.196832

to and stimulates biotinylation diffusely at the cytoplasm and nucleus (Fig. 5A). Consistent with this localization, the proximity interactors of CCDC66-RD consist of cytoplasmic and nuclear proteins (Fig. 5B; Table S1), which is in contrast to the profile of CCDC66 proximity interactors. Taken together, these results suggest that defects in satellite localization and function contribute to the retinal degeneration phenotype.

CCDC66 is required for efficient ciliogenesis and centriolar satellite distribution

The cellular functions of CCDC66 are not known. Physical and proximity interactions of CCDC66 to proteins that function in ciliogenesis (i.e. CEP72, CEP290 and PCM1) suggest that CCDC66 could have a similar function. By depleting CCDC66 in RPE1 cells, we tested whether CCDC66 is required for efficient ciliogenesis. Transfection with small interfering RNA (siRNA) against CCDC66 resulted in effective depletion after 72 h, as verified by western blotting of siRNA-transfected cells (Fig. 6A). Depletion of CCDC66 significantly (P<0.001) reduced cilium formation in serum-starved RPE1 cells (Fig. 6B), and this phenotype was rescued by expression of siRNA-resistant GFP–CCDC66-RR, which was verified by western blotting of siRNA-transfected RPE1 cells stably expressing GFP or GFP–CCDC66-RR (Fig. 6C; Fig. S4B). In cells where ciliogenesis phenotype was rescued, GFP–CCDC66-RR prominently localized to the cilium and also to satellites in a subset of cells (Fig. S4A), suggesting that ciliary and satellite localization of CCDC66 is important for its function during ciliogenesis. The ciliogenesis phenotype was not due to a defect in cell cycle progression, since both control and CCDC66-depleted cells had similar cell cycle profiles as analyzed by flow cytometry (Fig. S4E).

Because centriolar satellite organization and function is essential for ciliogenesis (Wang et al., 2016), we assessed the effects of CCDC66 depletion on these processes. Depletion of CCDC66 resulted in a significant (P<0.001) decrease in the amount of pericentrosomal PCM1 and a corresponding increase in cytoplasmic centriolar satellites, as determined by quantitative immunofluorescence (Fig. 6D,E). While CCDC66 depletion resulted in a significant (P<0.01) reduction in the amount of centriolar satellite-associated CEP290 (Fig. 6F,G), CEP290 depletion resulted in a significant (P<0.01) increase in the amount of pericentrosomal GFP–CCDC66 (Fig. 6I,J) and PCM1 (Fig. S4F, G). Both PCM1 and CEP290 redistribution phentoypes was rescued by expression of siRNA-resistant GFP–CCDC66-RR (Fig. 6E,G; Fig. S4A). The redistribution of centriolar satellites and altered localization of PCM1, CEP290 or CCDC66 was not due to the reduction in the protein levels of these proteins (Fig. 6A,H).

Given the interaction between CCDC66 and CEP290, we next determined the effect of CCDC66 and CEP290 codepletion on centriolar satellite organization. Interestingly, co-depletion of CCDC66 and CEP290 rescued the satellite redistribution phenotypes caused by individual CCDC66 and CEP290 depletions (Fig. S4F,G), suggesting that CEP290 and CCDC66 have opposing roles in satellite distribution in cells.

Given that CCDC66 binds to microtubules, we assessed whether it is required for the maintenance of a radial microtubule array in control and CCDC66-depleted cells by staining for microtubules (Fig. S4C). Control cells (72±2.9%, n=150) had significantly (P<0.05) higher percentage of centrosomally-organized radial arrays than CCDC66-depleted cells (45±5.2%, mean±s.e.m.; n=150) (Fig. S4D). This result indicates that CCDC66 plays a role in maintaining a stable microtubule array and that satellite redistribution phenotypes could be due to these organization changes

CCDC66 is required for relocalization of BBS4 from centriolar satellites to primary cilia during ciliogenesis

During ciliogenesis, the BBSome-associated protein BBS4 relocalizes from centriolar satellites to primary cilia (Kim et al., 2004, 2008; Nachury et al., 2007), and CCDC66 also has a similar localization pattern. PCM1, CEP290 and CEP72 were suggested to cooperate with BBS4 to promote ciliogenesis (Kim et al., 2008; Lopes et al., 2011; Stowe et al., 2012). Given the relationship of CCDC66 to these proteins, we assessed the effect of its depletion on the localization of BBS4 using the RPE1 cell line that stably expresses LAP–BBS4 (Nachury, 2008). Since ciliogenesis was decreased in CCDC66-depleted cells, we assayed BBS4 relocalization in the cells that formed cilia. A significant reduction (P<0.01) in the fraction of cilia containing LAP–BBS4 relative to control ciliated cells (73±3.7%, mean±s.e.m., of total) was observed for cells depleted of CCDC66 (37±2.5% of total) (Fig. 7A,B). In these cells, LAP–BBS4 remained associated with centriolar satellites rather than localizing to the cilium (Fig. 7A). Thus, disruption of centriolar satellite function by depletion of CCDC66 results in a failure of BBS4 recruitment to the cilium. Interestingly, we have not detected any interaction between CCDC66 and BBS4, neither in the BioID-pulldown of CCDC66 (Table S1) nor in the co-immunoprecipitation experiments (data not shown), suggesting that CCDC66 indirectly functions in relocalization of BBS4 to the cilium.

DISCUSSION

Centriolar satellites play important roles in a multitude of centrosome- and cilium-mediated cellular processes and are implicated in ciliopathies (Tollenaere et al., 2015). Interestingly, a significant number of centrosome and cilium complex proteins, including the ciliopathy-associated proteins CEP290, BBS4 and OFD1, localize to centriolar satellites. While these findings identify satellites as ubiquitous and essential structures for regulating the vertebrate centrosome and cilium complex, the molecular and functional relationship of the satellites to the centrosome and cilium complex and ciliopathies remain poorly understood. In this study, we characterized the retinal degeneration protein CCDC66 in ciliated retinal epithelial cells.

CCDC66 point mutation in dogs and null mutations in mouse were previously implicated in retinal degeneration, a phenotype that is common to ciliopathies (Dekomien et al., 2010; Gerding et al., 2011). We first identified CCDC66 as a proximity partner for known centriolar satellite proteins including CEP72, which interacts with CEP290 and functions in cilium formation and ciliary targeting of the BBSome complex (Stowe et al., 2012). Supporting this proximity relationship, CCDC66 colocalizes with PCM1 in cells, the canonical component of centriolar satellites and a significant percentage of the proximity partners for CCDC66 are components of the centriolar satellites and the centrosome and cilium complex. Using co-immunoprecipitation experiments, we showed that CCDC66 interacts with CEP290 and PCM1, but not with CEP72, suggesting that proximity relationship of CCDC66 to CEP72 does not reflect physical interaction. Like CCDC66, CEP290 was previously implicated in retinal degeneration in human ciliopathies and mouse models (Chang et al., 2006).

Remarkably, CCDC66 relocalizes from centriolar satellites to the primary cilium in ciliated cells and thus acts like BBS4, the BBSome component that localizes to satellites and is added last

Journal of Cell Science (2017) 130, 1450-1462 doi:10.1242/jcs.196832

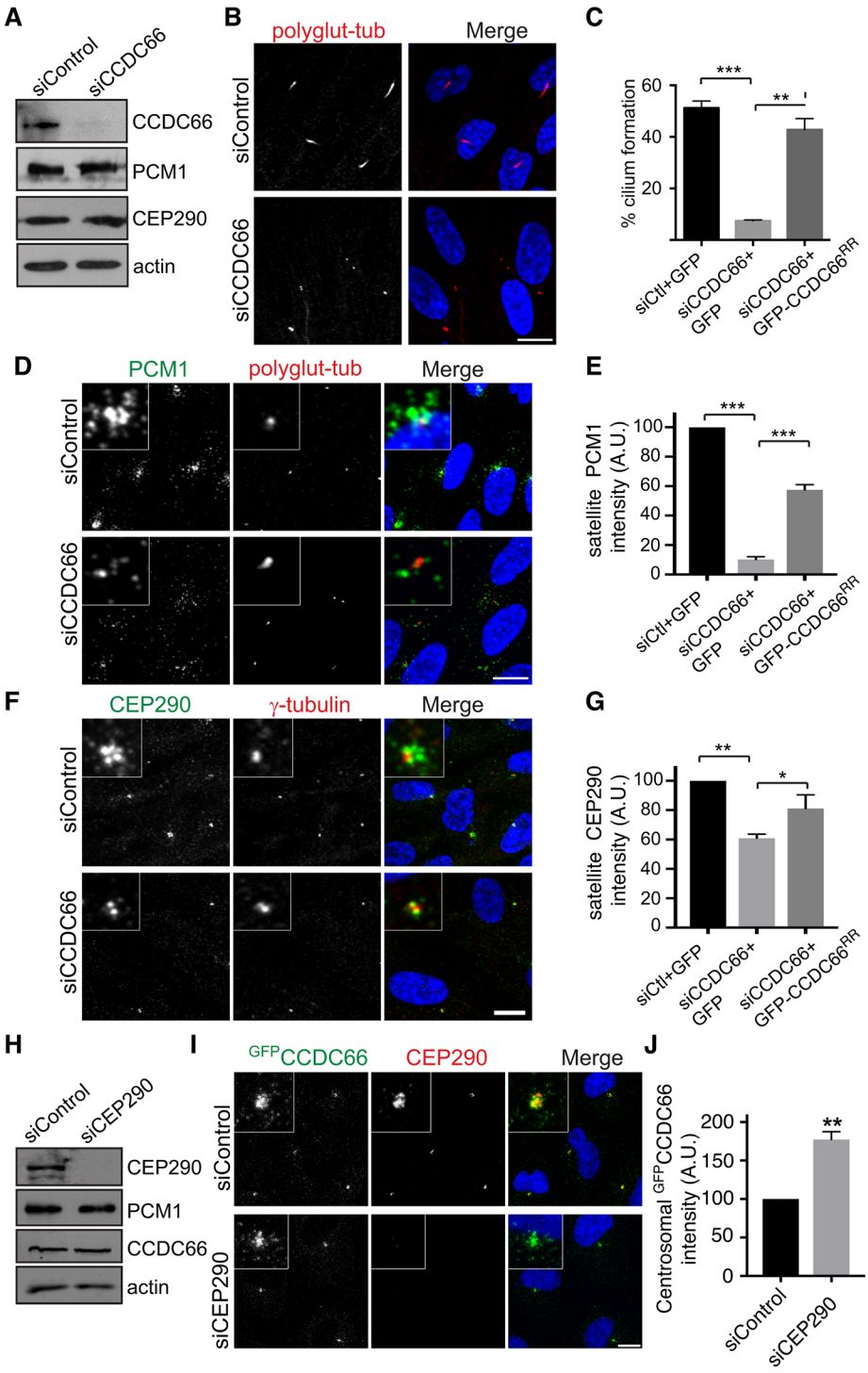

Fig. 6. See next page for legend.

during BBSome assembly (Nachury et al., 2007). This finding identifies CCDC66 as the only reported PCM1-associated protein other than BBS4 with such a localization pattern, suggesting that redistribution of proteins between the centriolar satellites and primary cilium is a common theme in ciliary trafficking. Interestingly, we did not identify CCDC66 as a component of the BBSome complex in BioID experiments. By analogy to BBS4 functions in cells (Kim et al., 2004; Nachury et al., 2007), it is possible that CCDC66 is part of a new ciliary complex that functions in ciliary trafficking. Future studies are required to address the functional significance of CCDC66 localization in ciliated cells.

We identified CCDC66 as a microtubule-associated protein by using *in vitro* and *in vivo* assays, and this is in agreement with a previous microtubule transcriptome screen in *Xenopus tropicalis* eggs (Sharp et al., 2011). Overexpression of CCDC66 in cells induced formation of microtubule bundles, disrupted centriolar satellite organization and inhibited ciliogenesis. Interestingly, endogenous CEP290 was recruited to these microtubule bundles,

Journal of Cell Science (2017) 130, 1450-1462 doi:10.1242/jcs.196832

Fig. 6. CCDC66 regulate cilium formation and centriolar satellite distribution. (A) CCDC66 siRNA effectively depletes CCDC66. RPE1 cells were transfected with control siRNA (siControl) or CCDC66 siRNA (siCCDC66), and 72 h after transfection extracts from cells were immunoblotted for CCDC66, CEP290, PCM1 and actin (loading control). (B) Effect of CCDC66 depletion on cilium formation. RPE1 cells were fixed 72 h after transfection with control siRNA or CCDC66 siRNA, and the percentage of ciliated cells was determined by staining for glutamylated tubulin and DAPI. (C) Quantification of rescue experiments. For rescue experiments, RPE-1 cells stably expressing GFP or GFP–CCDC66^{RR} were transfected with control and CCDC66 siRNAs. At 72 h post transfection cells were fixed, stained and quantified. *n*=300 cells for each sample, from three independent experiments. An ANOVA test was used for statistical analysis. (D) Effect of CCDC66 depletion on centriolar satellite organization. RPE1 cells were fixed 72 h after transfection with control siRNA or CCDC66 siRNA, and satellite organization was determined by staining for PCM1 and polyglutamylated tubulin and with DAPI. Images represent cells from the same coverslip taken with the same camera settings. (E) Quantification of rescue experiments. *n*=50 cells for each sample, from two independent experiments. ANOVA test was used for statistical analysis. (F) Effect of CCDC66 depletion on the pericentrosomal level of CEP290. RPE1 cells were fixed 72 h after transfection with control siRNA or CCDC66 siRNA, and stained for endogenous CEP290, γ-tubulin and with DAPI. (G) Quantification of rescue experiments. *n*=50 cells for each sample, from two independent experiments. ANOVA test was used for statistical analysis. (H) CEP290 siRNA (siCEP290) effectively depletes CEP290. RPE1 cells stably expressing GFP–CCDC66 were transfected with control siRNA or CEP290 siRNA, and 72 h after transfection extracts from cells were immunoblotted for CCDC66, CEP290, PCM1 and actin. (I) Effect of CEP290 depletion on the pericentrosomal level of GFP–CCDC66. RPE1 cells stably expressing GFP–CCDC66 were fixed 72 h after transfection with control siRNA or CEP290 siRNA, and satellite organization was determined by staining for GFP and CEP290 and with DAPI. (J) Quantification of I. Pericentrosomal GFP–CCDC66 fluorescence intensity was measured for control and CEP290-depleted cells and levels are normalized to 100. *n*=50 cells for each sample, from the independent experiments. A *t*-test was used for statistical analysis. Data in C,E,G and J represent mean±s.e.m. from two or three experiments per condition, **P*<0.05, ***P*<0.01, ****P*<0.001. A.U., arbitrary units. Scale bars: 10 µm, all insets show 4× enlarged centrosomes. ^{GFP}CCDC66 indicates stable expression of the fusion protein.

suggesting that CCDC66 might be required for association of CEP290 with microtubules. These results support the function of CCDC66 in localization and/or trafficking of proteins like CEP290 to and along microtubules.

A significant number of centriolar satellite protein identified to date have been implicated in cilium formation and function (Tollenaere et al., 2015). In cells depleted for CCDC66, there was a significant defect in ciliogenesis and PCM1- and CEP290-positive puncta did not cluster around the centrosome but were instead distributed throughout the cytosol. Defects in ciliogenesis could be a result of the defects in satellite function due to their redistribution in cells. Given that satellite organization and function depends on an intact microtubule network, it is possible that CCDC66 mediates the interaction between satellites and the cytoplasmic microtubule array, analogous to what has been reported for CEP290 (Kim et al., 2008), BBS4 (Kim et al., 2004) and PAR6α (Kodani et al., 2010). Taken together, our results support the role of centriolar satellites in cilium formation.

Centriolar satellites were shown to be important for efficient ciliogenesis because they control the entry of proteins to the cilium either by sequestering them or by trafficking them to or away from the cilium. For example, centriolar satellites sequester BBS4 and regulate recruitment of the BBSome complex to the cilium by limiting the amount of BBS4 available for incorporation into ciliary BBSomes (Stowe et al., 2012). Consistent with this model, we demonstrated that ciliary recruitment of BBS4 is compromised when CCDC66 is depleted. Our results support the role of centriolar satellites in the assembly of BBS4 into the BBSome complex and its subsequent ciliary recruitment. It is likely that CCDC66 regulates ciliary entry of the BBSome complex by interacting with microtubules and forming a complex with CEP290 at the satellites.

To determine how mutations in the *CCDC66* gene affect its function, we determined the localization and the proximity partners of the truncated form of CCDC66 (CCDC66-RD), which mimics the mutated protein found in dogs affected with retinal degeneration (Dekomien et al., 2010). CCDC66-RD localizes diffusely to the nucleus and cytosol and its proximity partners are almost all nuclear and cytoplasmic proteins. Moreover, CCDC66-RD does not interact with microtubules. These results suggest that defects in satellite localization and microtubule-binding contribute to the retinal degeneration phenotype.

In photoreceptor cells, the outer segment represents a highly modified cilium that contains visual transduction cascade components. The outer segment is connected to the inner segment by the connecting cilium, which resembles the ciliary transition zone. Phototransduction proteins are synthesized in the inner segment and transported to the outer segment through the connecting cilium (Wheway et al., 2014). Almost one-quarter of known retinal degeneration genes are associated with ciliary structure or function, including the BBSome complex (Wright et al., 2010) and the transition zone component CEP290 (Chang et al., 2006). Given the possible role of CCDC66 in ciliary trafficking, perturbation of this function could lead to photoreceptor degeneration through mislocalization of proteins required for phototransduction. Previous studies reported localization of CCDC66 to the inner segments of photoreceptor cells (Dekomien et al., 2010) and to the outer segment of rod cells (Gerding et al., 2011). Higher resolution localization studies in photoreceptor cells

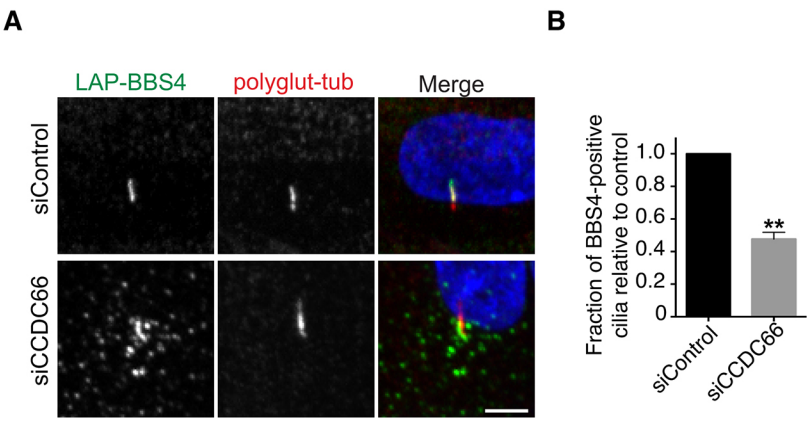

Fig. 7. CCDC66 regulates LAP–BBS4 recruitment to the cilium. (A) Effect of CCDC66 depletion on BBS4 relocalization from centriolar satellites to the primary cilium. RPE1 cells stably expressing LAP–BBS4 were fixed 72 h after transfection with control siRNA (siControl) or CCDC66 siRNA (siCCDC66), and LAP–BBS4 was visualized with anti-GFP antibody. Cells were also stained for polyglutamylated tubulin and with DAPI. Scale bar: 10 µm. (B) Quantification of results in A. Control siRNA-transfected levels were normalized to 1.0; *n*=50 cells for each sample, from three independent experiments. A *t*-test was used for statistical analysis. Data in B represent mean ±s.e.m. value from three experiments per condition, ***P*<0.01.

Journal of Cell Science (2017) 130, 1450-1462 doi:10.1242/jcs.196832

are required to determine whether the localization of to the centrosome and cilium complex and/or microtubules in RPE1 cells reflects localization in photoreceptor cells.

While *CCDC66* point and null mutations cause retinal degeneration in dogs and mouse, mutations have not yet been mapped to the *CCDC66* gene in human ciliopathies. There have been discrepancies between human ciliopathies and their respective mouse models, which are likely due to differences in species and/or functional nature of the mutation (Hall et al., 2013; Jiang et al., 2008; Mykytyn et al., 2004; Won et al., 2011). For most ciliopathies, mouse models fail to completely recapitulate the human phenotype. Therefore the loss-of-function phenotype of CCDC66 *in vivo* in humans is not known.

MATERIALS AND METHODS

Cell culture and transfection

hTERT-immortalized retinal pigment epithelial (RPE-1; ATCC CRL-4000) and LAPBBS4-hTERT-RPE1 cells were grown in DMEM/F12 (1:1; Invitrogen) supplemented with 10% fetal bovine serum (FBS; Atlanta Biologicals, Lawrenceville, GA). Human embryonic kidney (HEK293T; ATCC CRL-3216) cells were grown in DMEM supplemented with 10% FBS. All cells were cultured at 37°C and 5% CO_2. All cell lines were authenticated by Multiplex Cell line Authentication (MCA) and were tested for mycoplasma contamination by using the MycoAlert Mycoplasma Detection Kit (Lonza).

RPE1 cells were transfected with the plasmids by using Lipofectamine LTX (Invitrogen). HEK293T cells were transfected with the plasmids using 1 µg/µl polyethylenimine, molecular mass 25 kDa (PEI, Sigma-Aldrich, St. Louis, MO). For microtubule depolymerization experiments, cells were treated with 10 µg/ml nocodazole (US Biological, Swampscott, MA) for 3 h at 37°C. RPE1 cells stably expressing GFP–CCDC66, GFP–CCDC66-RR or GFP were generated by infection of cells with GFP–CCDC66-, GFP–CCDC66-RR- and GFP-expressing lentivirus. Lentivirus were generated as described previously (Mahjoub et al., 2010), by using pLVPT2-GFP-N1-CCDC66, pLVPT2-N1-CCDC66^{RR} and pLVPT2-N1 plasmids as transfer vectors.

Plasmids

Full-length cDNAs of CCDC66 (BC132827.1) and CEP290 (BC172566.1) were obtained from the DF/HCC DNA Resource Core (Harvard Medical School, MA). peGFP-N1-PCM1 and peGFP-N1-CEP72 plasmids were used for PCM1 (GenBank NM_006197) and CEP72 (GenBank NM_018140) amplification. The open reading frames (ORFs) of CEP72 and CCDC66/CCDC66 were amplified by PCR and N-terminally tagged with BirA* by cloning into pcDNA3.1-mycBioID. The ORFs of CCDC66/CCDC66 and CEP290 were amplified by PCR and cloned into pDONR221 using the Invitrogen Gateway system. Subsequent Gateway recombination reactions using pCS2+6xMyc DEST, pcDNA-DEST47 (Invitrogen) and pLVPT2-GFP-N1 were used to generate GFP–CEP290, GFP–CCDC66 and Myc–CCDC66. Deletion constructs of CCDC66 were made by PCR amplification of the indicated regions. PCR products were cloned into pDONR221 and gateway recombination reactions using pcDNA-DEST47 and pCS2+6xMyc DEST were used to produce GFP-tagged and Myc-tagged deletion constructs. The siRNA-resistant CCDC66 clone (CCDC66-RR) was generated by making five consecutive synonymous base pair changes in the center of the siRNA-targeted region (bold) by using overlapping PCR with the primers 5′-TTAGAAAAAGAAAACAATCG-GTGTAATGACCAGTG**C**AA**C**CA**A**TT**T**ACAAGAATAGAGAAACA-AACAAAACACATGAAGA-3′ and 5′- TCTTCATGTGTTTTGTTTGT-TTCTCTATTCTTGT**A**AA**T**TG**G**TT**G**CACTGGTCATTACACCGATT-GTTTTCTTTTTCTAA-3′. PCR products were cloned into pDONR221 and gateway recombination reactions using pcDNA-DEST47 and pLVPT2-GFP-N1 were used to produce GFP–CCDC66-RR.

siRNA and rescue experiments

CCDC66 was depleted using an siRNA with the sequence 5′-CAGTGTAATCAGTTCACAAtt-3′. Silencer Select Negative Control No. 1 (Thermo Scientific) was used as a control. CEP290 depletion was carried out using ON-TARGET Plus SMARTpool (Thermo Scientific). siRNAs were transfected into RPE1-hTERT cells with Lipofectamine RNAiMax according to the manufacturer's instructions (Thermo Fisher Scientific). For rescue experiments, RPE-1 cells stably expressing GFP or GFP–CCDC66-RR were transfected with control and CCDC66 siRNAs by using Lipofectamine RNAiMax (Thermo Fisher Scientific). At 72 h post transfection with the siRNAs, cells were fixed and stained.

Antibodies

Anti-PCM1 antibody was generated and used for immunofluorescence as previously described (Firat-Karalar et al., 2014). Other antibodies used for immunofluorescence were rabbit anti-CCDC66 (A303-339A; Bethyl Laboratories, Inc.) or mouse anti-CCDC66 (SAB1408484; Sigma-Aldrich) at 1:750, goat anti-PCM1 (sc-50164; Santa Cruz Biotechnology) at 1:1000, mouse anti-γ-tubulin (GTU-88; T5326; Sigma-Aldrich) at 1:4000, mouse anti-GFP (3e6; A-11120; Invitrogen) at 1:750, mouse anti-Myc (9e10; M4439; Sigma-Aldrich) at 1:500, rabbit anti-CEP290 (ab84870; Abcam) at 1:1000 and mouse anti-polyglutamylated tubulin (GT335; AG-20B-0020-C100; Adipogen) at 1:500. Antibodies used for western blotting were rabbit anti-CCDC66 (sc-102420; Santa Cruz Biotechnology) and rabbit anti-Myc (sc-789; Santa Cruz Biotechnology) at 1:2000, rabbit anti-CEP290 (ab84870; Abcam) at 1:1000, rabbit anti-CEP72 (19928-1-AP; Proteintech), rabbit anti-GFP at 0.15 µg/ml [as previously described in Hatch et al. (2010)], rabbit anti-PCM1 (19856-1-AP; Proteintech) at 1:1000 and rabbit anti-p38 MAPK (sc-535; Santa Cruz Biotechnology) at 1:2000.

Immunoprecipitation and BioID pulldowns

For the co-immunoprecipitation experiments, HEK293T cells were transiently transfected, incubated for 24 h, washed with PBS, and lysed in lysis buffer (50 mM Tris-HCl pH 7.4, 266 mM NaCl, 2.27 mM KCl, 1.25 mM KH_2PO_4, 6.8 mM Na_2HPO_4-$7H_2O$ and 1% NP-40, protease inhibitors). Insoluble material was pelleted, and soluble material was incubated with goat anti-GFP antibodies (Rockland) and then with protein A beads (Affi-Prep). Beads were washed in lysis buffer, eluted in sample buffer and run on SDS-PAGE gels. BioID streptavidin pulldown was performed as described previously (Firat-Karalar et al., 2014).

Microtubule pelleting assays

Purified bovine brain tubulin was diluted to a concentration of 2 mg/ml in BRB80 buffer (80 mM PIPES, pH 6.8, 1 mM $MgCl_2$, 1 mM EGTA including protease inhibitors, 1 mM GTP, 1 mM dithiothreitol and 20 µM taxol), precleared at 90,000 rpm (~350,000 ***g***) for 5 min at 4°C and brought to a final concentration of 20 µM Taxol in a step-wise manner at 37°C. 0.5 nmol of MBP–CCDC66 fragments affinity purified from E. coli, or 1.5 mg cell extracts were diluted in a 250 µl final volume of BRB80, cleared at 90,000 rpm (~350,000 ***g***) for 5 min at 4°C. Protein samples were mixed with taxol-stabilized microtubules or buffer control and incubated for 30 min at 30°C. Samples were loaded onto 40% glycerol BRB80 cushions and centrifuged at 55,000 rpm (~250,000 ***g***) for 10 min. Supernatant and pellet fractions were separated by SDS-PAGE for analysis.

Mass spectrometry and data analysis

Mass spectrometry analysis was done as described previously with the following change (Firat-Karalar et al., 2014): The MS/MS spectra were searched with the ProLuCID algorithm against the Uniprot human database (downloaded on 20 March 2014). For each BioID experiment, data were derived from three biological replicates. Control data were derived from mock-transfected and BirA*-transfected HEK293T cells. To compare data across different runs and assess the abundance of each proximity partner, we applied a normalization of spectral counts (Zybailov et al., 2006). Individual spectral count values were normalized against the sum of all spectral counts for a particular run, resulting in an normalized spectral abundance factor (NSAF). For presentation purposes, we multiplied each NSAF value by 100. To distinguish the nonspecific interactors, we calculated the ratio of the NSAF of each identified protein to the NSAF of the corresponding proteins

Journal of Cell Science

in the control datasets. A protein was considered to be a contaminant if the ratio was smaller than 2.5. For analysis of the data from three independent BioID experiments, we only accounted for the proteins that were identified in at least two independent experiments and that have a spectral count greater than four.

Immunofluorescence, microscopy and quantification

For immunofluorescence experiments, cells were grown on coverslips and fixed in either methanol or 4% paraformaldehyde in PBS. After rehydration in PBS, cells were blocked in 3% BSA (Sigma-Aldrich) in PBS plus 0.1% Triton X-100. Coverslips were incubated in primary antibodies diluted in blocking solution, and Alexa Fluor 488-, 594-, or 680-conjugated secondary antibodies were diluted in 1:500 in blocking solution (Invitrogen). Biotinylated proteins were detected with Alexa Fluor 594-coupled streptavidin (1:500; Invitrogen). Samples were mounted using Mowiol. Coverslips of cells were imaged using LAS X software (Premium; Leica) on a scanning confocal microscope (SP8; Leica Microsystems) with Plan Apofluar 63×1.4 NA objective and by spinning disk confocal microscopy using a Zeiss Axiovert with a Yokogawa CSU-10 confocal head using a cooled charge-coupled device camera (Orca ER, Hamamatsu Photonics; Cascade EM-CCD, Photometrics). For deconvolved images, Huygens Deconvoluation software was used.

Quantitative immunofluorescence for PCM1 and CEP290 was performed by acquiring a *z*-stack of control and depleted cells using identical gain and exposure settings. The *z*-stacks were used to assemble maximum-intensity projections. The centrosome region was defined by γ-tubulin staining in each cell and its fluorescence pixel intensity was measured in a circular 3 μm^2 area centered on the centrosome. The satellite region was defined as the 19 μm^2 ring around the centrosome. Quantifications and image processing were performed using ImageJ (National Institutes of Health, Bethesda, MD). Background was quantified by measuring fluorescence intensity of a region of equal dimensions in the area neighboring the centrosome and the satellites. Primary cilium formation was assessed by counting the total number of cells and the number of cells with primary cilia.

Statistical analysis

Statistical significance and *P* values were assessed by one-way analysis of variance and Student's *t*-tests using Prism software (GraphPad Software, La Jolla, CA). Error bars reflect s.e.m. Following key is followed for asterisk placeholders for *P*-values in the figures: **P*<0.05, ***P*<0.01, ****P*<0.001.

Acknowledgements

We acknowledge the Stearns laboratory and David Mick for insightful discussions regarding this work. LAP-BBS4 RPE1 cells were a kind gift from Maxence Nachury (Stanford University, Stanford, CA).

Competing interests

The authors declare no competing or financial interests.

Author contributions

E.N.F.-K. and D.C. designed the experiments and wrote the manuscript. E.N.F.-K., D.C., E.C. and E.O. carried out the majority of the experiments. N.R. and J.R.Y. carried out mass spectrometry analyses of the BioID pulldowns.

Funding

This work was supported by European Research Council (StG679140), Türkiye Bilimsel ve Teknolojik Araştirma Kurumu (TUBITAK) (214Z223), an Feyzi Akkaya Research Fund for Scientific Activities (FABED) Eser Tümen Research Award, a Türkiye Bilimler Akademisi (Turkish Academy of Sciences) Distinguished Young Scientist Award to (E.N.F.-K.), and the National Institutes of Health (grant P41 GM103533 to J.R.Y.). Deposited in PMC for release after 12 months.

Supplementary information

Supplementary information available online at
http://jcs.biologists.org/lookup/doi/10.1242/jcs.196832.supplemental

References

Adams, N. A., Awadein, A. and Toma, H. S. (2007). The retinal ciliopathies. *Ophthalmic Genet.* **28**, 113-125.

Barenz, F., Mayilo, D. and Gruss, O. J. (2011). Centriolar satellites: busy orbits around the centrosome. *Eur. J. Cell Biol.* **90**, 983-989.

Berbari, N. F., O'Connor, A. K., Haycraft, C. J. and Yoder, B. K. (2009). The primary cilium as a complex signaling center. *Curr. Biol.* **19**, R526-R535.

Betleja, E. and Cole, D. G. (2010). Ciliary trafficking: CEP290 guards a gated community. *Curr. Biol.* **20**, R928-R931.

Bettencourt-Dias, M., Hildebrandt, F., Pellman, D., Woods, G. and Godinho, S. A. (2011). Centrosomes and cilia in human disease. *Trends Genet.* **27**, 307-315.

Chang, B., Khanna, H., Hawes, N., Jimeno, D., He, S., Lillo, C., Parapuram, S. K., Cheng, H., Scott, A., Hurd, R. E. et al. (2006). In-frame deletion in a novel centrosomal/ciliary protein CEP290/NPHP6 perturbs its interaction with RPGR and results in early-onset retinal degeneration in the rd16 mouse. *Hum. Mol. Genet.* **15**, 1847-1857.

Dekomien, G., Vollrath, C., Petrasch-Parwez, E., Boevé, M. H., Akkad, D. A., Gerding, W. M. and Epplen, J. T. (2010). Progressive retinal atrophy in Schapendoes dogs: mutation of the newly identified CCDC66 gene. *Neurogenetics* **11**, 163-174.

Firat-Karalar, E. N. and Stearns, T. (2015). Probing mammalian centrosome structure using BioID proximity-dependent biotinylation. *Methods Cell Biol.* **129**, 153-170.

Firat-Karalar, E. N., Rauniyar, N., Yates, J. R., III and Stearns, T. (2014). Proximity interactions among centrosome components identify regulators of centriole duplication. *Curr. Biol.* **24**, 664-670.

Follit, J. A., Tuft, R. A., Fogarty, K. E. and Pazour, G. J. (2006). The intraflagellar transport protein IFT20 is associated with the Golgi complex and is required for cilia assembly. *Mol. Biol. Cell* **17**, 3781-3792.

Gerding, W. M., Schreiber, S., Schulte-Middelmann, T., de Castro Marques, A., Atorf, J., Akkad, D. A., Dekomien, G., Kremers, J., Dermietzel, R., Gal, A. et al. (2011). Ccdc66 null mutation causes retinal degeneration and dysfunction. *Hum. Mol. Genet.* **20**, 3620-3631.

Gupta, G. D., Coyaud, É., Gonçalves, J., Mojarad, B. A., Liu, Y., Wu, Q., Gheiratmand, L., Comartin, D., Tkach, J. M., Cheung, S. W. T. et al. (2015). A dynamic protein interaction landscape of the human centrosome-cilium interface. *Cell* **163**, 1484-1499.

Hall, E. A., Keighren, M., Ford, M. J., Davey, T., Jarman, A. P., Smith, L. B., Jackson, I. J. and Mill, P. (2013). Acute versus chronic loss of mammalian Azi1/Cep131 results in distinct ciliary phenotypes. *PLoS Genet.* **9**, e1003928.

Hatch, E. M., Kulukian, A., Holland, A. J., Cleveland, D. W. and Stearns, T. (2010). Cep152 interacts with Plk4 and is required for centriole duplication. *J. Cell Biol.* **191**, 721-729.

Hildebrandt, F., Benzing, T. and Katsanis, N. (2011). Ciliopathies. *N. Engl. J. Med.* **364**, 1533-1543.

Hodges, M. E., Scheumann, N., Wickstead, B., Langdale, J. A. and Gull, K. (2010). Reconstructing the evolutionary history of the centriole from protein components. *J. Cell Sci.* **123**, 1407-1413.

Jiang, S.-T., Chiou, Y.-Y., Wang, E., Lin, H.-K., Lee, S.-P., Lu, H.-Y., Wang, C.-K. L., Tang, M.-J. and Li, H. (2008). Targeted disruption of Nphp1 causes male infertility due to defects in the later steps of sperm morphogenesis in mice. *Hum. Mol. Genet.* **17**, 3368-3379.

Kim, S. and Dynlacht, B. D. (2013). Assembling a primary cilium. *Curr. Opin. Cell Biol.* **25**, 506-511.

Kim, K. and Rhee, K. (2011). The pericentriolar satellite protein CEP90 is crucial for integrity of the mitotic spindle pole. *J. Cell Sci.* **124**, 338-347.

Kim, J. C., Badano, J. L., Sibold, S., Esmail, M. A., Hill, J., Hoskins, B. E., Leitch, C. C., Venner, K., Ansley, S. J., Ross, A. J. et al. (2004). The Bardet-Biedl protein BBS4 targets cargo to the pericentriolar region and is required for microtubule anchoring and cell cycle progression. *Nat. Genet.* **36**, 462-470.

Kim, J., Krishnaswami, S. R. and Gleeson, J. G. (2008). CEP290 interacts with the centriolar satellite component PCM-1 and is required for Rab8 localization to the primary cilium. *Hum. Mol. Genet.* **17**, 3796-3805.

Kim, K., Lee, K. and Rhee, K. (2012). CEP90 is required for the assembly and centrosomal accumulation of centriolar satellites, which is essential for primary cilia formation. *PLoS ONE* **7**, e48196.

Kodani, A., Tonthat, V., Wu, B. and Sutterlin, C. (2010). Par6 alpha interacts with the dynactin subunit p150 Glued and is a critical regulator of centrosomal protein recruitment. *Mol. Biol. Cell* **21**, 3376-3385.

Kodani, A., Yu, T. W., Johnson, J. R., Jayaraman, D., Johnson, T. L., Al-Gazali, L., Sztriha, L., Partlow, J. N., Kim, H., Krup, A. L. et al. (2015). Centriolar satellites assemble centrosomal microcephaly proteins to recruit CDK2 and promote centriole duplication. *Elife* **4**, e07519.

Krupp, M., Marquardt, J. U., Sahin, U., Galle, P. R., Castle, J. and Teufel, A. (2012). RNA-Seq Atlas–a reference database for gene expression profiling in normal tissue by next-generation sequencing. *Bioinformatics* **28**, 1184-1185.

Lee, J. Y. and Stearns, T. (2013). FOP is a centriolar satellite protein involved in ciliogenesis. *PLoS ONE* **8**, e58589.

Lopes, C. A. M., Prosser, S. L., Romio, L., Hirst, R. A., O'Callaghan, C., Woolf, A. S. and Fry, A. M. (2011). Centriolar satellites are assembly points for proteins implicated in human ciliopathies, including oral-facial-digital syndrome 1. *J. Cell Sci.* **124**, 600-612.

Luders, J. and Stearns, T. (2007). Microtubule-organizing centres: a re-evaluation. *Nat. Rev. Mol. Cell Biol.* **8**, 161-167.

Mahjoub, M. R., Xie, Z. and Stearns, T. (2010). Cep120 is asymmetrically localized to the daughter centriole and is essential for centriole assembly. *J. Cell Biol.* **191**, 331-346.
Martinez-Garay, I., Rustom, A., Gerdes, H.-H. and Kutsche, K. (2006). The novel centrosomal associated protein CEP55 is present in the spindle midzone and the midbody. *Genomics* **87**, 243-253.
Mykytyn, K., Mullins, R. F., Andrews, M., Chiang, A. P., Swiderski, R. E., Yang, B., Braun, T., Casavant, T., Stone, E. M. and Sheffield, V. C. (2004). Bardet-Biedl syndrome type 4 (BBS4)-null mice implicate Bbs4 in flagella formation but not global cilia assembly. *Proc. Natl. Acad. Sci. USA* **101**, 8664-8669.
Nachury, M. V. (2008). Tandem affinity purification of the BBSome, a critical regulator of Rab8 in ciliogenesis. *Methods Enzymol.* **439**, 501-513.
Nachury, M. V., Loktev, A. V., Zhang, Q., Westlake, C. J., Peränen, J., Merdes, A., Slusarski, D. C., Scheller, R. H., Bazan, J. F., Sheffield, V. C. et al. (2007). A core complex of BBS proteins cooperates with the GTPase Rab8 to promote ciliary membrane biogenesis. *Cell* **129**, 1201-1213.
Nigg, E. A. and Raff, J. W. (2009). Centrioles, centrosomes, and cilia in health and disease. *Cell* **139**, 663-678.
Pampliega, O., Orhon, I., Patel, B., Sridhar, S., Diaz-Carretero, A., Beau, I., Codogno, P., Satir, B. H., Satir, P. and Cuervo, A. M. (2013). Functional interaction between autophagy and ciliogenesis. *Nature* **502**, 194-200.
Roux, K. J., Kim, D. I. and Burke, B. (2013). BioID: a screen for protein-protein interactions. *Curr. Protoc. Protein Sci.* **74**, Unit 19 23.
Scholey, J. M. (2008). Intraflagellar transport motors in cilia: moving along the cell's antenna. *J. Cell Biol.* **180**, 23-29.
Sharp, J. A., Plant, J. J., Ohsumi, T. K., Borowsky, M. and Blower, M. D. (2011). Functional analysis of the microtubule-interacting transcriptome. *Mol. Biol. Cell* **22**, 4312-4323.
Silva, E., Betleja, E., John, E., Spear, P., Moresco, J. J., Zhang, S., Yates, J. R., III, Mitchell, B. J. and Mahjoub, M. R. (2016). Ccdc11 is a novel centriolar satellite protein essential for ciliogenesis and establishment of left-right asymmetry. *Mol. Biol. Cell* **27**, 48-63.
Staples, C. J., Myers, K. N., Beveridge, R. D. D., Patil, A. A., Lee, A. J. X., Swanton, C., Howell, M., Boulton, S. J. and Collis, S. J. (2012). The centriolar satellite protein Cep131 is important for genome stability. *J. Cell Sci.* **125**, 4770-4779.
Staples, C. J., Myers, K. N., Beveridge, R. D. D., Patil, A. A., Howard, A. E., Barone, G., Lee, A. J. X., Swanton, C., Howell, M., Maslen, S. et al. (2014). Ccdc13 is a novel human centriolar satellite protein required for ciliogenesis and genome stability. *J. Cell Sci.* **127**, 2910-2919.
Stowe, T. R., Wilkinson, C. J., Iqbal, A. and Stearns, T. (2012). The centriolar satellite proteins Cep72 and Cep290 interact and are required for recruitment of BBS proteins to the cilium. *Mol. Biol. Cell* **23**, 3322-3335.
Tang, Z., Lin, M. G., Stowe, T. R., Chen, S., Zhu, M., Stearns, T., Franco, B. and Zhong, Q. (2013). Autophagy promotes primary ciliogenesis by removing OFD1 from centriolar satellites. *Nature* **502**, 254-257.
Tollenaere, M. A. X., Mailand, N. and Bekker-Jensen, S. (2015). Centriolar satellites: key mediators of centrosome functions. *Cell. Mol. Life Sci.* **72**, 11-23.
van der Horst, A., Simmons, J. and Khanna, K. K. (2009). Cep55 stabilization is required for normal execution of cytokinesis. *Cell Cycle* **8**, 3742-3749.
Villumsen, B. H., Danielsen, J. R., Povlsen, L., Sylvestersen, K. B., Merdes, A., Beli, P., Yang, Y.-G., Choudhary, C., Nielsen, M. L., Mailand, N. et al. (2013). A new cellular stress response that triggers centriolar satellite reorganization and ciliogenesis. *EMBO J.* **32**, 3029-3040.
Vitre, B. D. and Cleveland, D. W. (2012). Centrosomes, chromosome instability (CIN) and aneuploidy. *Curr. Opin. Cell Biol.* **24**, 809-815.
Wang, W.-J., Tay, H. G., Soni, R., Perumal, G. S., Goll, M. G., Macaluso, F. P., Asara, J. M., Amack, J. D. and Bryan Tsou, M.-F. (2013). CEP162 is an axoneme-recognition protein promoting ciliary transition zone assembly at the cilia base. *Nat. Cell Biol.* **15**, 591-601.
Wang, L., Lee, K., Malonis, R., Sanchez, I. and Dynlacht, B. D. (2016). Tethering of an E3 ligase by PCM1 regulates the abundance of centrosomal KIAA0586/Talpid3 and promotes ciliogenesis. *Elife* **5**, e12950.
Waters, A. M. and Beales, P. L. (2011). Ciliopathies: an expanding disease spectrum. *Pediatr. Nephrol.* **26**, 1039-1056.
Wheway, G., Parry, D. A. and Johnson, C. A. (2014). The role of primary cilia in the development and disease of the retina. *Organogenesis* **10**, 69-85.
Won, J., Marin de Evsikova, C., Smith, R. S., Hicks, W. L., Edwards, M. M., Longo-Guess, C., Li, T., Naggert, J. K. and Nishina, P. M. (2011). NPHP4 is necessary for normal photoreceptor ribbon synapse maintenance and outer segment formation, and for sperm development. *Hum. Mol. Genet.* **20**, 482-496.
Wright, A. F., Chakarova, C. F., Abd El-Aziz, M. M. and Bhattacharya, S. S. (2010). Photoreceptor degeneration: genetic and mechanistic dissection of a complex trait. *Nat. Rev. Genet.* **11**, 273-284.
Zybailov, B., Mosley, A. L., Sardiu, M. E., Coleman, M. K., Florens, L. and Washburn, M. P. (2006). Statistical analysis of membrane proteome expression changes in Saccharomyces cerevisiae. *J. Proteome Res.* **5**, 2339-2347.